# Regional Characteristics for Interpreting Inverted Echo Sounder (IES) Observations

ZACHARIAH R. HALLOCK

*Naval Ocean Research and Development Activity, Physical Oceanography Branch, National Space Technology Laboratories, MS 39529*

(Manuscript received 11 April 1986, in final form 24 November 1986)

ABSTRACT

Changes in round-trip acoustic travel time ($\tau$) measured between a bottom moored inverted echo sounder and the sea surface can be interpreted as changes in dynamic height ($D$) with suitable calibration information. The $\tau$, $D$, and isotherm and isopycnal depths ($Z$) have been calculated using hydrographic (CTD) data from three regions: the Norwegian Current, the Sargasso Sea and the eastern Gulf Stream. Regressions of $D$ and $Z$ on $\tau$ were performed. The slope for the Norwegian Current is $-1.70 \pm 0.01$ [dyn cm (m s)$^{-1}$], for the Sargasso Sea $-3.89 \pm 0.16$ [dyn cm (m s)$^{-1}$] and for the Gulf Stream $-3.13 \pm 0.07$ [dyn cm (m s)$^{-1}$]. The quasi-random scatter about regression curves is found to be primarily the result of variability in the seasonal thermocline, where present.

## 1. Introduction

The inverted echo sounder (IES; Bitterman and Watts, 1979) is a bottom moored, upward-looking acoustic device for measuring the round-trip acoustic travel time ($\tau$) between the sea surface and bottom. Fluctuations in the height of the sea surface have a measurable effect on $\tau$ (1 ms m$^{-1}$, Watts and Rossby, 1977) but the dominant factor by far is variability of the second-speed profile in the intervening water column. For example, a change in the thermal structure corresponding to a change in dynamic height ($D$) of 100 dynamic centimeters (dcm) results in a change in $\tau$ of about 30 ms in the Gulf Stream region (equivalent to about a 600 m change in thermocline depth). The IES is thus well suited for the study of mesoscale baroclinic variability. If the IES is also provided with a precision pressure sensor (Watts and Wimbush, 1981), the combined measurements yield both barotropic and baroclinic components of variability in the surface pressure field.

Interpreting changes in IES measured $\tau$ as changes in $D$ (or pycnocline depth) requires supporting information about the sound-speed and density profiles in the region where the IES is to be deployed. This information can be obtained from hydrographic observations at IES sites wherever practicable and/or from statistics of historical hydrographic data from the region of interest. The study described in this report is an example of the latter.

Calculations of $\tau$, $D$, and isotherm and isopycnal depths were made using hydrographic (CTD) profile data acquired in three regions where mesoscale features were present: the southeastern Norwegian Sea (NS), the eastern Gulf Stream (GS) south of New England, and the Sargasso Sea (SS) east of Jacksonville, Florida. The results are based exclusively on these data (no actual IES data are included).

## 2. Background

The attempt to use bottom-mounted inverted echo sounders (IESs) to monitor changes in the depth of the main thermocline was first made by Rossby (1969). Using two hydrographic datasets, he compared calculated round-trip acoustic travel time ($\tau$) with the depths of the 10° and 12°C isotherms and found remarkable correlations. A linear least-squares slope of about 20 m (ms)$^{-1}$ was found. He subsequently conducted an eight-day experiment near Bermuda, where he found that measured $\tau$ was quite stable, varying only in response to surface and internal tides. During MODE, several bottom-moored IESs were deployed to monitor thermocline depth fluctuations. There were simultaneous hydrographic (CTD) observations in the area. Watts and Rossby (1977) summarized the MODE results and formally examined the relationship between $\tau$ and $D$. They found that fluctuations in $D$ could be inferred from $\tau$ changes with an uncertainty of only $\pm 1$ dcm. To arrive at this estimate, they intercompared $\tau$ from the IES with $\tau$ and $D$ calculated from CTD data. These calculations were done across the main thermocline between 500 and 1500 m, which excluded the surface layers. Comparisons of measured $\tau$ with the depth of the 10°C isotherm (thermocline depth) showed a rms scatter of about 5 m, which scales to about 0.7 dcm in $D$. Thermocline depth varies as $D$, provided the first baroclinic mode dominates the variability. They also calculated $\tau$ and $D$ between the surface and 4000 m, using historical hydrographic data from the Gulf Stream region, and obtained an

rms uncertainty of 5 dyn cm about a linear, least-squares fit.

## 3. CTD data analysis

### a. Approach

Changes in $D$ and $\tau$ are calculated from profiles of specific volume ($\alpha$), and reciprocal sound speed ($\gamma$), which are functions of pressure ($P$), temperature ($T$) and salinity ($S$). Integrating in pressure coordinates

$$D' = -\int_{P_1}^{P_2} \alpha' dP \tag{1}$$

$$\tau' = -\frac{2}{g}\int_{P_1}^{P_2} (\alpha\gamma)' dP, \tag{2}$$

where $D = \bar{D} + D'$, $\tau = \bar{\tau} + \tau'$; the overbar denotes a local time average.

The integrands of (1) and (2) are of similar form and the arguments presented by Watts and Rossby (1977) demonstrate how $D'$ and $\tau'$ are nearly linearly related. The relationship between $D'$ and $\tau'$ depends on hydrographic conditions in the vicinity of an IES mooring, and ideally, we should like to have a series of hydrographic profiles at each IES site to provide stable statistics. In a region such as the Gulf Stream, which varies on time scales ranging from several days to several months, this is not practical. In such a region, however, variability is primarily due to lateral shifting of horizontal gradients and the necessary statistics can be obtained by quasi-synoptic sampling over the region surrounding the IESs. There are seasonal warming and cooling effects which may be missed with this approach, but the synoptic-scale data can be complemented by representative XBT and/or AXBT surveys throughout the year.

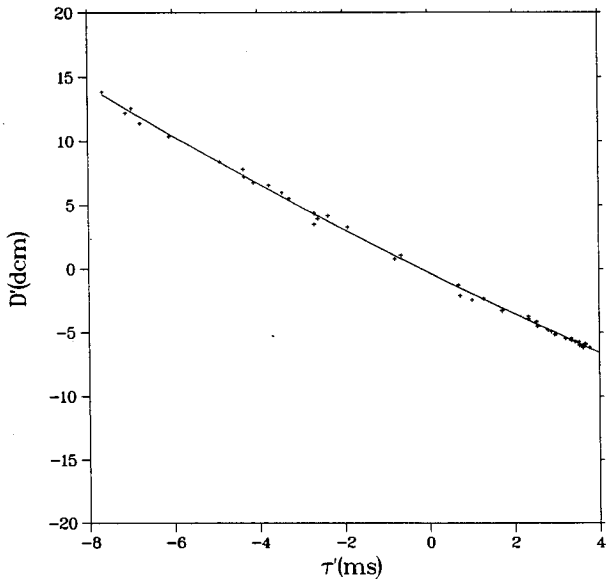


FIG. 1. $D'$ vs $\tau'$, with superimposed quadratic regression curve, calculated with CTD profiles from the Norwegian Current, between 20 and 1000 db.

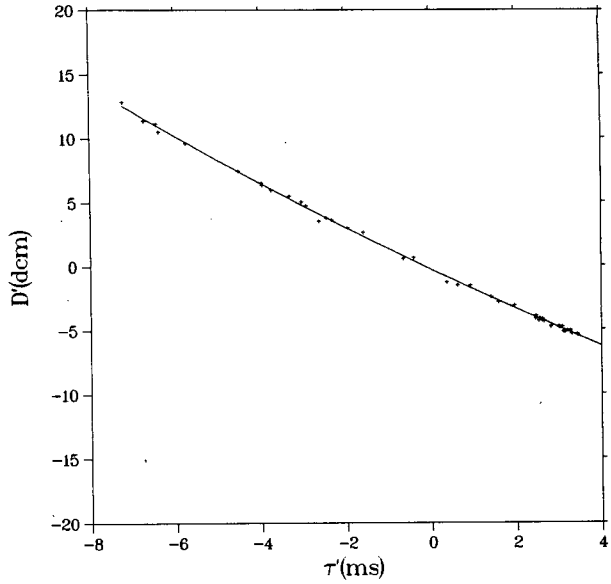


FIG. 2. As in Fig. 1 but between 100 and 1000 db.

In the analysis to follow, CTD data from three regions are examined, $D'$, $\tau'$, and, in some cases, isopleth depths are calculated and linear regressions are performed. Sources of uncertainties and scatter in the regressions are discussed.

### b. Description of the data

Area 1 is the southeastern Norwegian Sea (NS), and the data consist of 48 CTD casts to about 1100 m, taken in three sections across the Norwegian Current. This current is the extension of the North Atlantic Current and transports Atlantic water northward through the Faeroe–Shetland Channel to mix with waters of Arctic and Subarctic origin. The data were acquired in March 1981 when no seasonal thermocline was observed. The velocity of the Norwegian Current was about 25 cm $s^{-1}$ from the surface to a depth of about 300 m. (These data were obtained by the Naval Oceanographic Office (NOO) and have been part of NORDA's archives.)

Area 2 is the western Sargasso Sea (SS) near 30°N, 71°W. Data consist of a grid of about 30 CTDs to 2000 m, separated by about 20 nautical miles (n mi), acquired in September 1979. The area contained an anticyclonic eddy with velocities of the order of 20 cm $s^{-1}$ (Hallock et al., 1981) and there was a well-developed seasonal thermocline near 60 m. The source of these data is the same as for Area 1.

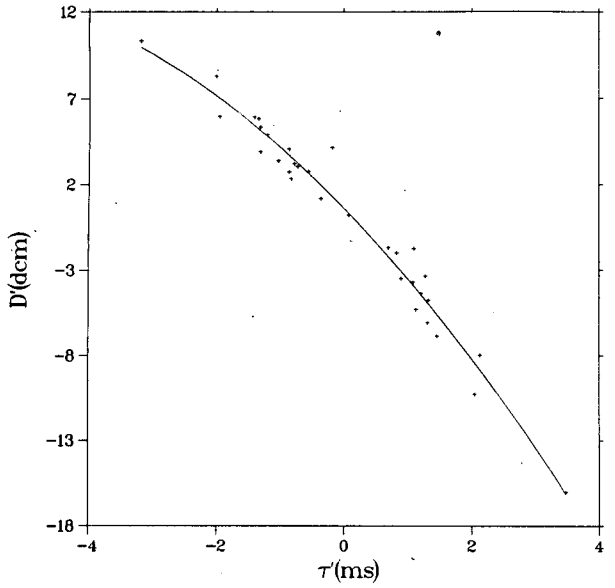


FIG. 3. As in Fig. 1 but calculated with 32 CTD profiles from the Sargasso Sea between 12 and 1950 db.

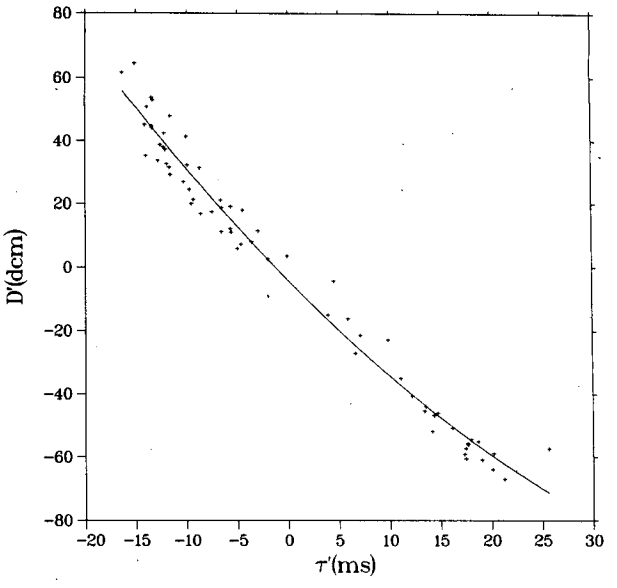


FIG. 5. As in Fig. 1 but calculated with 66 CTD profiles from the Gulf Stream between 3 and 3000 db.

Area 3 consists of 66 CTD casts from the eastern Gulf Stream region (GS) in the vicinity of the New England Seamounts. The data are distributed in sections across and along the Gulf Stream and most extend to the bottom. A seasonal thermocline was present at most locations in and south of the Stream. There were strong frontal features near the northern boundary of the current. These data were acquired by the Woods Hole Oceanographic Institution in summer 1983, and are described by Hogg et al. (1985).

### c. *Calculations*

For each of the three datasets, $D'$ and $\tau'$ were computed by integrating Eqs. (1) and (2) over selected pressure intervals. The pressure limits ($P_1$ and $P_2$) were chosen to include the maximum number of profiles, and yet get close to the surface as well as below most of the baroclinic variability. A second set of calculations was done of $D'$ and $\tau'$ where the upper pressure limit was chosen deliberately to exclude the upper layer and seasonal thermocline, where present. $D'$ is plotted as a

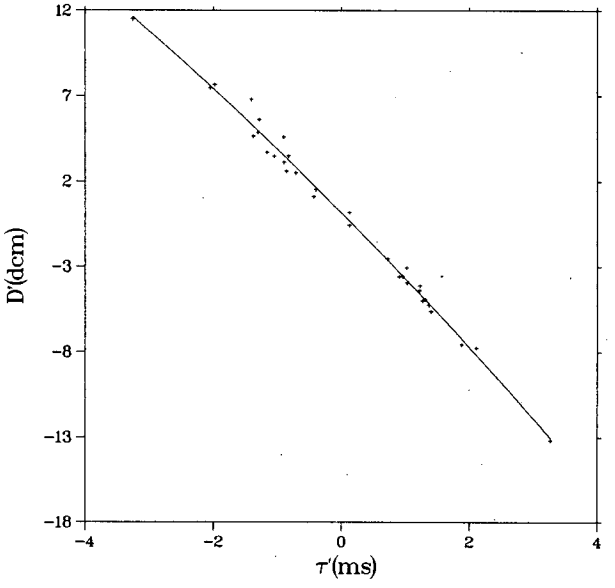


FIG. 4. As in Fig. 3 but between 200 and 1950 db.

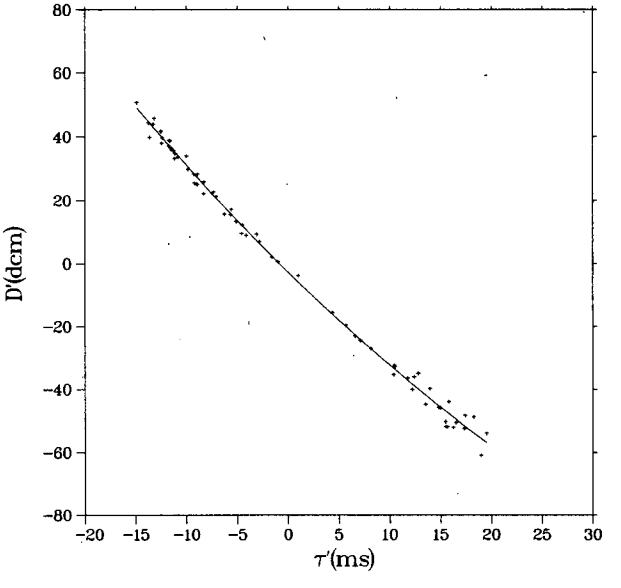


FIG. 6. As in Fig. 5 but between 200 and 3000 db.

TABLE 1. Linear regression of $D'$ on $\tau'$.

| Case | $n$ | $P_1 - P_2$ | rms $\tau'$ (ms) | rms $D'$ (dcm) | $r$ | $E_L$ (dcm) | $B_l \pm \delta B_l$ (dcm ms$^{-1}$) |
|---|---|---|---|---|---|---|---|
| NS-1 | 46 | 20–1000 | 3.74 | 6.39 | −.998 | ±0.36 | −1.70 ± .014 |
| NS-2 | 46 | 100–1000 | 3.45 | 5.72 | −.999 | ±0.30 | −1.65 ± .013 |
| SS-1 | 32 | 12–1950 | 1.468 | 5.86 | −.976 | ±1.29 | −3.89 ± .156 |
| SS-2 | 32 | 200–1950 | 1.453 | 5.52 | −.995 | ±0.56 | −3.78 ± .068 |
| GS-1 | 66 | 3–3000 | 12.69 | 40.22 | −.986 | ±6.70 | −3.13 ± .065 |
| GS-2 | 66 | 200–3000 | 11.51 | 35.67 | −.997 | ±2.77 | −3.09 ± .029 |

function of $\tau'$ in Figs. 1–6 where quadratic regression curves have been superimposed.

Linear ($_l$) and quadratic ($_q$) regressions of $D'$ and $\tau'$ and error estimate ($E$) were computed as follows:

$$D_l = B_l\tau' + C_l \quad \text{(linear)}$$

$$E_l = \text{rms}(D' - D_l)$$

$$D_q = A_q\tau'^2 + B_q\tau' + C_q \quad \text{(quadratic)}$$

$$E_q = \text{rms}(D' - D_q).$$

The uncertainty in the linear slope, $B_l$, is given by $B_l = E_l/[N^{1/2}\text{rms}(\tau')]$ where $N$ is the number of observations.

Results of the regression calculations for $D'$ vs $\tau'$ are summarized in Tables 1 and 2 (since $D'$ and $\tau'$ are anomalies, $C_l = 0$ and is not shown). Linear regressions were also done for selected isotherm and isopycnal depths vs $\tau'$ and these results are shown in Table 3.

### d. Discussion

It is apparent in all cases that a significant correlation exists between $D'$ and $\tau'$. Indeed, the values of $r$ are all greater than 0.97. The departures from a perfect linear fit fall into two categories: a general curvature which can be corrected for with a quadratic fit, and a quasi-random residual scatter.

The NS area data yields the best fit of $D'$ and $\tau'$, and case NS-2 shows very little improvement over NS-1. A significant seasonal thermocline is absent and near-surface variability is that of salinity in a thin (10 m) layer. The slope, $B_l$, is about half the values found in the other two regions due to a significantly different $T$–$S$ relationship.

The SS data exhibits the lowest value of $r$. The variability of $D'$ is comparable to that in NS, but the signal-to-noise ratio is lower. There is a well-developed seasonal thermocline, as well as a subsurface maximum of density variability near 40 m. The value of $E_l$ is slightly greater than that given by Watts and Rossby (1977) for the same region. Exclusion of the upper 200 m (Case SS-2) reduces $E_l$ and improves the fit dramatically.

Signal levels in the GS area data are about eightfold greater than in the other areas. The $E_l$ is larger than for SS but $r$ is considerably higher, indicating a higher signal-to-noise ratio. A seasonal thermocline is present in and south of the Gulf Stream and a subsurface maximum in density variability extends from about 35 to 65 m. Case GS-2 reduces $E_l$ by about one half and improves the fit significantly.

The results of the quadratic regressions show a general improvement for all cases. This improvement is due to the accommodation of the small but systematic curvature in $D'$ vs $\tau'$. The curvature effect is estimated by $A_q\tau'^2$ (which is numerically equal to $C_q$, since $\tau'$ and $D'$ have zero mean) and is of the same order as $E_q$, the rms error of the quadratic fit. A statistical test ($F$-Test) shows that significant improvement results with the quadratic term for all six cases. The improvement is marginal, however, for SS-2. In the NS cases, the curvature effect is nearly negligible. In both the GS and SS cases, however, the curvature effect as well as $E_q$ are considerably reduced by calculating $D'$ and $\tau'$

TABLE 2. Quadratic regression of $D'$ on $\tau'$.

| Case | $n$ | $P_1 - P_2$ | $A_q$ (dcm ms$^{-2}$) | $B_q$ (dcm ms$^{-1}$) | $C_q$ (dcm) | $E_q$ (dcm) |
|---|---|---|---|---|---|---|
| NS-1 | 46 | 20–1000 | .0215 | −1.65 | −0.29 | 0.28 |
| NS-2 | 46 | 100–1000 | .0253 | −1.60 | −0.29 | 0.19 |
| SS-1 | 32 | 12–1950 | −.280 | −3.84 | 0.58 | 1.07 |
| SS-2 | 32 | 200–1950 | −.080 | −3.78 | 0.16 | 0.53 |
| GS-1 | 66 | 3–3000 | .0253 | −3.27 | −4.01 | 6.23 |
| GS-2 | 66 | 200–3000 | .0203 | −3.17 | −2.66 | 2.26 |

TABLE 3. Linear regression of $Z_T$, $Z_\sigma$ on $\tau'$.

| Case | rms $Z'$ (m) | $r$ | $E_L$ (m) | $B_l \pm \delta B_l$ (m ms$^{-1}$) |
|---|---|---|---|---|
| NS | | | | |
| $T$ = 3°C | 139 | −.994 | 15.2 | −35.2 ± 0.6 |
| $\sigma_t$ = 27.88 (3°) | 138 | −.991 | 19.0 | −35.8 ± 0.8 |
| SS | | | | |
| $T$ = 15°C | 45.9 | −.946 | 15.18 | −29.5 ± 1.8 |
| 12°C | 33.7 | −.982 | 6.40 | −22.5 ± 0.8 |
| 10°C | 37.3 | −.961 | 10.5 | −24.3 ± 1.3 |
| $\sigma_t$ = 27.02 (12°) | 35.1 | −.982 | 6.78 | −23.4 ± 0.8 |
| GS | | | | |
| $T$ = 15°C | 252 | −.991 | 33.2 | −20.1 ± 0.3 |
| 12°C | 270 | −.992 | 34.5 | −21.0 ± 0.3 |
| 10°C | 270 | −.996 | 23.4 | −21.1 ± 0.2 |
| $\sigma_t$ = 27.29 (10°) | 258 | −.995 | 24.4 | −20.1 ± 0.2 |

below the thermocline, but the slopes $B_l$, $B_q$ do not change significantly. The source of the curvature, which does not always have the same sign, is a result of the nonlinearities of both the equation of state and the $T$–$S$ relationship.

In cases where the first baroclinic mode dominates variability, dynamic height changes are reflected in isotherm and isopycnal depth changes in the main thermocline. When IES data are used for monitoring positions of strong mesoscale features or where a two-layer description is sought, a direct interpretation of $\tau'$ as changes in thermocline depth ($Z_T$) or pycnocline depth ($Z_\sigma$) may be useful. Correlations between $Z_T$, $Z_\sigma$, and $\tau'$ (Table 3; the isopycnals selected correspond approximately to the isotherms indicated by the temperature in parentheses) are generally lower than those for $D'$ and $\tau'$. This is partly because $Z_T$, $Z_\sigma$ are likely to be noisier quantities than $D'$ (an integral) and partly because events at some other depth may affect $\tau'$ but not a particular isotherm (or isopycnal).

For the SS case, $B_l(Z_{10})$ and $E_l(Z_{10})$ are 24 m (ms)$^{-1}$ and 10 m, respectively, which differ considerably from the 14 m (ms)$^{-1}$ and 4 m reported by Watts (1975), for the same region. This difference might be seasonal or regional (Watts' data was acquired in summer near 28°N, 69.5°W while the SS data was acquired in early fall, near 30°N, 71°W). For both GS and SS, $Z_T$ above the main thermocline is poorly correlated with $\tau'$; this observation may have implications for relations between near-surface and mesoscale (deep) variability. Results for $Z_T$ in the Norwegian Current are nearly the same for all isotherms. The vertical temperature gradient is nearly constant between the surface and the lower depth limit of the data, and salinity variability is low. In all cases, $Z_\sigma$, $\tau'$ has a slightly lower correlation than does $Z_T$, $\tau'$ at the corresponding isotherm. This is expected, since sound-speed fluctuations tend to follow temperature fluctuations more closely than do density fluctuations.

The $Z_3$ (NS), $Z_{12}$ (SS) and $Z_{10}$ (GS) have the highest correlations with $\tau'$ and are the most useful for interpreting IES observations. Also $Z_{12}$ and $Z_{15}$ have good correlations and are included since they have been used to define the thermocline by other investigators (e.g., Hansen, 1969; Watts and Johns, 1982; Watts and Tracey, 1985).

To determine possible effects of the lower pressure limit, $P_1$, calculations with a subset of the GS data which extended to 5000 db were performed between 12 and 3000 db and between 12 and 5000 db. There is very little difference between the results in these two cases.

The salient results to emerge from these calculations are the values of $B_l$ and their associated errors. They are the regional calibration factors for conversion of IES measured $\tau'$ into $D'$, $Z_T$ or $Z_\sigma$. The primary limitation to the accuracy of the $D'$ vs $\tau'$ regression for any given area appears to be variability in the upper 100–200 m of the water column.

### e. *Further analysis of scatter*

In cases where a seasonal thermocline is present, the upper 200 m is a major source of scatter in the $D'$ vs $\tau'$ relation. It is useful to explore further the nature of this scatter. The NS cases contain relatively little scatter and hence can serve as a control for comparison with the other two areas.

A linear relationship between $D'$ and $\tau'$ requires some similarity in the integrands of (1) and (2). A necessary (but not sufficient) condition is that profiles of rms ($\alpha'$) and rms [$(\alpha\gamma)'$] have the same shape. These profiles for the three regions are plotted in Figs. 7–9. There is a subsurface maximum in $\alpha'$ for both GS and SS, which is not present in $(\alpha\gamma)'$. This feature, which corresponds to the seasonal thermocline, gives rise to much of the scatter observed in the $D'$–$\tau'$ relationship. This is due to a different $T$–$S$ relationship in the upper layers, where salinity variations tend to change density in the same sense as temperature variations; i.e., $T$ and $S$ are noncompensating. No subsurface maximum in $\alpha'$ is present in NS; a thin layer of low salinity near the

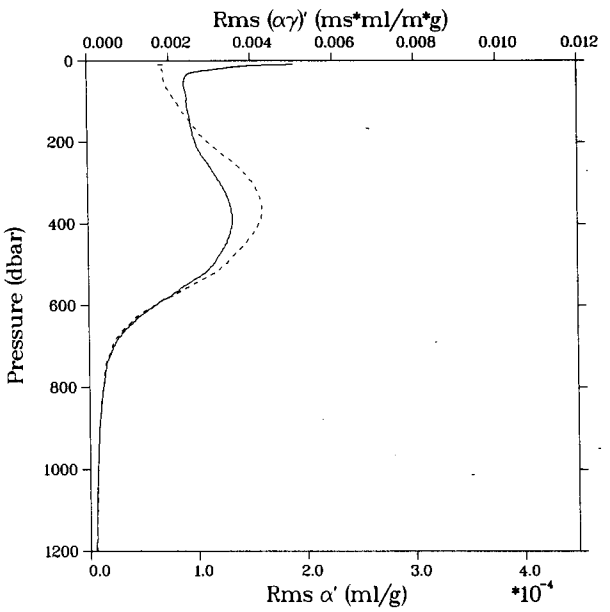


FIG. 7. Profiles of rms $\alpha'$ (solid) and rms $(\alpha\gamma)'$ (dashed) for 44 CTD profiles from the Norwegian Current.

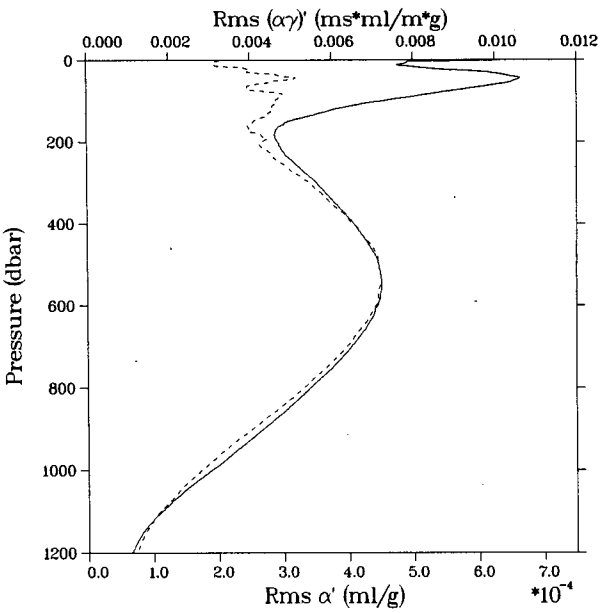


FIG. 9. As in Fig. 7 but for 66 CTD profiles from the Gulf Stream.

surface, a manifestation of the fresh Norwegian coastal water, has very little effect on the integral of $\alpha'$. The shallow variability in $\alpha$ does not appear to be correlated with the primary signal which corresponds to the variability in the main thermocline. This shallow variability is likely to be spatially and temporally aliased; it may be associated with internal waves or frontal fluctuations.

To better understand the effects of temperature and salinity variations on the $D'$, $\tau'$ relation, we focus attention on GS data and examine Eqs. (1) and (2) more closely. The integrands can be expanded about the mean to yield

$$\alpha' = \frac{\partial \alpha}{\partial T} T' + \frac{\partial \alpha}{\partial S} S' \tag{3}$$

$$(\alpha\gamma)' = \left(\alpha \frac{\partial \gamma}{\partial T} + \gamma \frac{\partial \alpha}{\partial T}\right) T' + \left(\alpha \frac{\partial \gamma}{\partial S} + \gamma \frac{\partial \alpha}{\partial S}\right) S'. \tag{4}$$

The corresponding integrals of (3) and (4) result in the respective components of $D'$ and $\tau'$:

$$D' = D_T + D_S$$

and

$$\tau' = \tau_{T1} + \tau_{T2} + \tau_{S1} + \tau_{S2} = \tau_T + \tau_S.$$

These quantities were computed for the GS data over three pressure intervals (3–3000, 3–200, 200–3000 db) and their statistics appear in Table 4. The dominant terms in the $D'$–$\tau'$ relation are $D'_T$, $D'_S$, and $\tau_{T1}$. Correlations are slightly higher among all terms for the 200–3000 db integral than for 3–3000 db. They are significantly lower for 3–200 db, indicating a different regime in this interval, as previously suggested.

In the deeper interval $D_S = -0.41 D_T$: the high negative correlation implies the effect of salinity variability is almost exactly opposed to that of temperature variability. Also in this interval, $\tau'_S \approx 0.07\tau_T$ and $\tau'_{T2} \approx -0.08\tau_{T1}$, showing the dominance of $\tau_{T1}$. In the shallower interval, correlations retain their signs but are significantly lower. $D_S \approx -0.52 D_T$, $\tau_S \approx 0.16\tau_T$ and $\tau_{T2} \approx -0.13\tau_{T1}$, showing the increased importance of salinity variability to $\tau'$. In all cases, $\tau_{S1} = \tau_{S2}$ with high correlation. The increased effect of salinity and

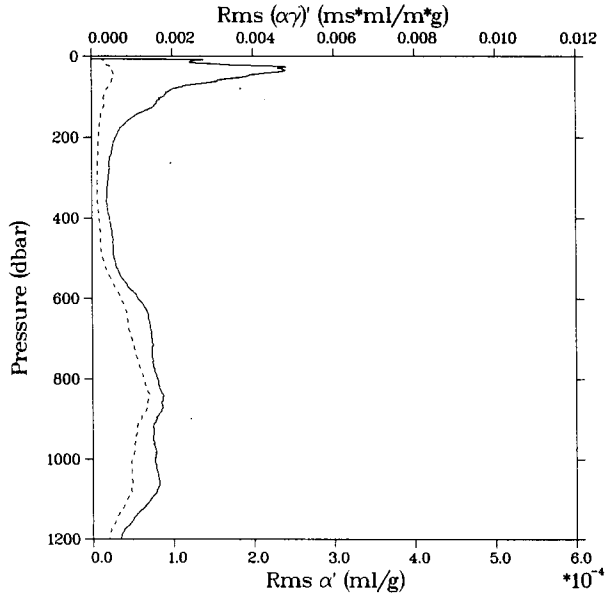


FIG. 8. As in Fig. 7 but for 32 CTD profiles from the Sargasso Sea.

TABLE 4. Statistics of components of $D'$ and $\tau'$ intervals computed from GS data [rms $D'$ (dcm) and rms $\tau'$ (ms)].

| $P_1$–$P_2$ (db): | 3–200 | 200–3000 | 3–3000 |
|---|---|---|---|
| $D'$ | 7.9 | 34 | 39 |
| $D_T$ | 15.1 | 63 | 76 |
| $D_S$ | 7.8 | 26 | 33 |
| $\tau'$ | 1.66 | 11.2 | 12.6 |
| $\tau_T$ | 1.34 | 10.2 | 11.3 |
| $\tau_S$ | 0.21 | 0.7 | 0.9 |
| $\tau_{T1}$ | 1.54 | 11.1 | 12.3 |
| $\tau_{T2}$ | 0.20 | 0.9 | 1.0 |
| $\tau_{S1}$ | 0.11 | 0.4 | 0.5 |
| $\tau_{S2}$ | 0.11 | 0.3 | 0.4 |
| Correlations between $\tau'$ and $D'$ components | | | |
| $D'\tau'$ | −.774 | −.997 | −.986 |
| $D_T D_S$ | −.917 | −.996 | −.994 |
| $D_T \tau_{T1}$ | −1.000 | −.999 | −.997 |
| $\tau_{T1}\tau_{T2}$ | −1.000 | −.999 | −.997 |
| $\tau_T \tau_S$ | .924 | .996 | .993 |
| $\tau_{S1}\tau_{S2}$ | 1.000 | 1.000 | 1.000 |

poorer $T$–$S$ correlation in the upper 200 m indicate that seasonal corrections based only on temperature profiles (e.g., XBTs) will have limitations in this interval.

## 4. Summary

The GS-2 and SS-2 cases simulate an extreme seasonal variation, since choosing $P1$ at 200 db is roughly equivalent to extending the $T$ and $S$ at 200 db to the surface. Hence, seasonal changes in $B_l$ of the order of those shown in Table 1 might be expected. Clearly, a study of year-round observations would provide more accurate estimates of seasonal variations.

If one is interested primarily in the dynamic signal in the main thermocline, as suggested in the calculations done by Watts (1975) (see section 2, this paper), $B_l$ for the deeper $P1$ might be used, with its better statistics, thus avoiding the seasonal variation. Furthermore, additional regression calculations with SS and GS data (not presented here) with $P1$ at 200 for $D'$, but with $P1$ remaining near the surface for $\tau'$, correlations are nearly as good (at least 0.991) as for SS-2 and GS-2. On the other hand, if the main interest is specifically in the dynamic height changes at the surface, some estimate of seasonal variations should be included when interpreting $\tau'$.

The most direct dynamical interpretation of IES travel-time data is as changes in dynamic height across the main thermocline, when mesoscale variability is present. The relationship is virtually linear and uncertainties are acceptably small in the three regions analyzed here. Comprehensive hydrographic surveys can provide the necessary statistics to effect the conversion of travel-time data to dynamic height change. These surveys may be concurrent with an IES deployment or comprised of historical data. They must be extensive enough to include all sets of hydrographic conditions that are likely to be experienced at the IES sites. The slopes and uncertainties for the NS, SS and GS regions are $-1.70 \pm 0.01$ (dcm ms$^{-1}$), $-3.89 \pm 0.16$ (dcm ms$^{-1}$) and $-3.13 \pm 0.07$ (dcm ms$^{-1}$), respectively. There is a small but significant quadratic dependence of $D'$ on $\tau'$. In applications where high precision is required, results such as those in Table 2 will be useful.

The inference of isotherm depth change from travel-time data depends more strongly on the assumption that the first baroclinic mode is dominant, which in SS and GS is likely to be a good assumption. For the isotherms which gave the best correlations with $\tau'$, the slopes and uncertainties for the NS ($Z_3$), SS ($Z_{12}$), GS ($Z_{10}$) are $-35.2 \pm 0.6$ (m ms$^{-1}$), $-22.5 \pm 0.8$ m ms$^{-1}$ and $-21.1 \pm 0.2$ m ms$^{-1}$, respectively.

The primary source of uncertainty in the conversion factor is relatively uncorrelated $T$–$S$ variability in the near surface layers when a seasonal thermocline is present. This variability is likely to be associated with local warming, frontal movement or internal waves, and is probably aliased in the data sets of this study. In future calibration studies, attention should be focused on the shallow effects with data, which are able to resolve the smaller scales.

*Acknowledgments.* I would like to thank Dr. Don Johnson and Mr. William Teague for their comments. This research was supported by the Office of Naval Research under Program Element 61153N and NORDA Project 3205 330.

### REFERENCES

Bitterman, D. S., and D. Randolph Watts, 1980: The inverted echo sounder. *IEEE OCEANS '79 Proc.*, September, San Diego, 1979.

Hallock, Z. R., W. J. Teague and R. D. Broome, 1981: A deep, thick isopycnal layer within an anticyclonic eddy. *J. Phys. Oceanogr.*, **11**(12), 1674–1677.

Hansen, D. V., 1970: Gulf Stream meanders between Cape Hatteras and the Grand Banks. *Deep-Sea Res.*, **17**, 495–511.

Hogg, Nelson G., Robert S. Pickart, Ross M. Hendry and William Smethie, 1985: On the northern recirculation gyre of the Gulf Stream. *Deep-Sea Res.*, **33**(9A), 1139–1166.

Rossby, H. Thomas, 1969: On monitoring depth variations of the main thermocline acoustically. *J. Geophys. Res.*, **74**, 5542–5546.

Watts, D. Randolph, 1975: Inverted echo sounder. Instrument Description and Intercomparison Report of the MODE-I Intercomparison Group (unpublished report), 149–163.

——, and W. E. Johns, 1982: Gulf Stream meanders: observations on propagation and growth. *J. Geophys. Res.*, **87**(C12), 9467–9476.

——, and H. Thomas Rossby, 1977: Measuring dynamic heights with inverted echo sounders: results from MODE. *J. Phys. Oceanogr.*, **7**, 345–358.

——, and K. L. Tracey, 1985: Objective analysis of the Gulf Stream thermal front from inverted echo sounders. *Proc. Gulf Stream Workshop*, West Greenwich, RI.

——, and Mark Wimbush, 1981: Sea surface height and thermocline depth variations measured from the sea floor. *Int. Symp. on Acoustic Remote Sensing of the Atmosphere and Oceans*, Calgary, Alberta.